New Materials, Compounds and Applications
Vol.9, No.3, 2025, pp.482-501
https://doi.org/10.62476/nmca.93482

EFFECT OF POMELO PEEL EXTRACT ON THE FORMATION OF IRON OXIDE BY GREEN SYNTHESIS AND ITS APPLICATION TO REMOVE CONGO RED AND BRILLIANT GREEN

Bich Ngoc Hoang[1*], Ngan Tran Thi Hong[2], Tran Thien Hien[1], Minh Anh Hoang[3]

[1]Institute of Applied Technology and Sustainable Development, Nguyen Tat Thanh University, Ho Chi Minh, Vietnam
[2]Faculty of Chemical Engineering and Food Technology, Nong Lam University, Ho Chi Minh, Vietnam
[3]Faculty of Biology and Biotechnology, University of Science, Vietnam National University, Ho Chi Minh, Vietnam

Abstract. α-Fe_2O_3 material was synthesized by a new green chemistry method extracted from pomelo with the characteristic structure, α-Fe_2O_3 shows the O↔Fe↔O functional group, the hexagonal crystal characteristics and the calculated crystal size is 72.16 nm. In addition, α-Fe_2O_3 was applied as an effective adsorbent to remove Congo Red and Brilliant Green dyes as organic dyes from aqueous solution. Best adsorption conditions of α-Fe_2O_3 were recorded with CR: 60 minutes, temperature 50 ℃, pH8, dosage 1 g/L, concentration of 250 mg/L. Best adsorption conditions of α-Fe_2O_3 were recorded with BG: 30 minutes, temperature 30 ℃, pH4, dosage 3 g/L, concentration of 100 mg/L. The maximum absorption capacity under optimal conditions was 33.701 mg/g for BG and 130.700 mg/g for CR. The adsorption process was predicted to be mainly controlled by physical and chemical interactions on the monolayer adsorbent surface.

Keywords: *Pomelo peel, green synthesis, iron oxide, Congo Red, Brilliant Green.*

Corresponding Author: *Bich Ngoc Hoang, Institute of Applied Technology and Sustainable Development, Nguyen Tat Thanh University, Ho Chi Minh, Vietnam, e-mail: bichhn@ntt.edu.vn*

Received: *6 May 2025;* ***Accepted:*** *5 August 2025;* ***Published:*** *4 December 2025.*

1. Introduction

Life on Earth is maintained by three environmental factors: soil, water and air. Water plays a role in the living process of humans and the lives of many types of creatures on Earth. Due to human development rapid urbanization and industrialization, the water environment is gradually polluted by many different kinds of pollutants. Pollutants that are difficult to treat in the environment such as antibiotics, colorants, heavy metals and some other organic pollutants. Among them, pigments from the textile industry are considered difficult to handle because they involve the use of toxic pollutants, do not decompose and are easily absorbed by surface water, sediment and soil. Many methods have been used effectively in eliminating dyes. The methods divided into 3 large groups are biological, chemical and physical. Physical and chemical methods include adsorbent, catalyst, decomposition of adsorption catalysts, ozoneization, coagulation, electrical coagulation of electrochemical processes, membrane separation methods, ultrasound methods, Oxidation of wet air, liquid emulsion method, have successfully applied in the

treatment of different dyes (Chiavola, 2011; Fernández *et al*., 2010). Although it brings many benefits, the process of synthesizing the material creates many solvents that are toxic to the environment. To minimize negative impacts on the environment, the need to utilize by-products to create new materials and practical applications has been of interest and development to researchers for more than a decade. Since then a new synthetic method has been defined as "Green Chemistry".

In the method of synthesizing materials using green chemistry, green catalysts and green solvents are the most economical method. Currently, many researchers have paid attention to low -cost sources or take advantage of agricultural by -products to create green catalysts or green solvents (Clarke *et al*., 2018; Mutlu & Barner, 2022). In particular, products with high biological activity content or natural energy sources have been used such as solar energy, wind energy, water energy, pineapple peel, green tea leaves, orange peel, Lemon peel and pomelo peel. Taking advantage of green solvents helps the synthesis process avoid creating new pollutants. In recent years, research on nanomaterials or organic framework materials using green chemistry methods has been of interest to researchers (Gómez-López *et al*., 2020). Nanoparticles were synthesized mainly from plant extracts. Among them, Fe_2O_3 nanoparticles were widely studied due to their structural diversity when combined with plant extracts. In 2021, Sushmitha's group of authors synthesized Fe_2O_3 nanoparticles using Bauhinia tomentosa extract. The results show the formation of small Fe_2O_3 nanoparticles with a size of about 70 nm. The XRD spectrum also shows the formation of Fe_2O_3, besides there is still diffraction of substances with amorphous structure. This can be attributed to the contribution of the extract and is also shown in the FTIR spectrum (Lakshmnarayanan *et al*., 2021). In 2023, the research team of author Bahig A. Eldeeb synthesized a nano solution of Fe_3O_4 from Citrus Sinensis (sweet Orange) fruit peel. The results show that the material could be antibacterial and antioxidation and dye's decomposition. The structural results clearly show the formation of Fe_3O_4 with Face-Centered Cubic shape, about 19 nm in size. In which methylene blue was decomposed in 4 hours at a concentration of 2 mM with the decomposition efficiency about 50% (Eldeeb *et al*., 2023). In 2024, Fe_2O_3 nanoparticles were synthesized by Sithara's research team using orange peel extract. The results show that the nanoparticles were contained few impurities with the main components to be Fe, Oxygen and a particle size of 25-80 nm. FTIR spectrum also shows the existence of organic's groups believed to be in the orange peel extract (Sithara *et al*., 2024). In general, research on Fe_2O_3 materials were focused to antibacterial (Kanagasubbulakshmi & Kadirvelu, 2017), anti-oxidant (Bouafia *et al*., 2021), anti-inflammatory (Eldeeb *et al*., 2023; Mahmoudi *et al*., 2020) and some biological activities (Abbas *et al*., 2024; Abdullah *et al*., 2020; Bashir *et al*., 2020; Bouafia *et al*., 2021; Eldeeb *et al*., 2023; Jegadeesan *et al*., 2019; Mahmoudi *et al*., 2020; Nasiri, 2023; Ramesh *et al*., 2019; Sathishkumar *et al*., 2018). Besides, there were still quite limited studies on the treatment of dyes and antibiotics, heavy metal (Ali *et al*., 2017; Nguyen *et al*., 2020; Sithara *et al*., 2024).

Fe_2O_3 materials synthesized by green chemistry methods are still quite limited. In some studies, Pomelo, orange and lemon peels have been used to synthesize Fe_2O_3 materials (Bashir *et al*., 2020; Dehbi *et al*., 2020; Yarmohammadi *et al*., 2022). Pomelo of scientific name's is Citrus maxima, belongs to the Rutaceae family and the largest citrus fruit. Pomelo is a purebred variety of the citrus family with a main distribution in Southeast Asia with many pomelo varieties of high economic value (Van Hung *et al*., 2021). According to the food and agricultural organization (FAO), Vietnam has an output

of 1034 million tons with a part of growing 80,291 thousand hectares (accounting for about 22.2% of the developing area worldwide). The revenue of pomelo products has been collected for Vietnam from $ 644 million to $ 723 million from 2019 to 2021. Comes with large output, related products caused the manufacturing industry to release a large amount of PP. PP contains many natural compounds such as flavonoids, limonoids, alkaloids, chimpanzee Oil, pectin and organic acid. In which ingredients such as Limonene, 1-Octanol, 3,7-Dimethyl-1,6-Ectadien-3-ol (β-linalool), α-Tyrineol, 3.7-Dimethyl-6-olen-1-ol (Cis-Geraniol, β-Citral, Guariol (Lemonol), (E) -3,7-Dimethyl-2,6-Ctadienal (Kahrilas *et al*., 2014). The components in PP contain free functional groups like β-linalool, 1-ctanol contains OH group; Limonene, α-Tyrineol contains CH_3 and CH_2 groups; 6-Ctadienal contains CH_3 group and links C=O. These compounds contribute to solvents for synthesizing Fe_2O_3 materials. Using green solvents helps the synthesis process avoid producing new pollutants. Fe_2O_3 material after the synthesis is used to assess the adsorption or decomposition of organic dyes. In this study, α-Fe_2O_3 nanoparticles would be synthesized by green chemical method using PP extract. The affecting factors of the adsorption process were also evaluated. Kinetic and isotherm models were used to predict the processor adsorbent mechanism that could take place between materials and dyes.

2. Experimental Methods

Pretreatment and Chemicals

For the PP extract with a low impurity content, PP were pre-treated before the extraction process. PP were washed (remove dirt and damaged parts), dried at 50 ^oC for 48 hours (remove water) and crushed into powder. Several chemicals and dyes were used to synthesise and evaluate the material's adsorption. Iron (III) chloride hexahydrate ($FeCl_3 \cdot 6H_2O$), Sodium hydroxide (NaOH) and ethanol (≥ 95% purity) were produced by Xilong Scientific Co., Ltd. Methyl Blue (MB), Brilliant Green (BG), Congo Red (CR) and Methyl Red (MR) were produced by Sigma-Aldrich Co, Switzerland.

Preparation of extracted PP and synthesis α-Fe_2O_3

Extracted from PP: Organic compounds in PP were extracted through the soaking method and showed in Figure 1A. 1 gram of PP powder was added in Erlenmeyer with 15 ml of 70% ethanol. The mixture was impregnated for 24 hours, at 30 ^oC. The extracted solution was filtered in a Buchner flask. The PP extract was in tube samples in a refrigerator at 10 ± 5 ^oC.

Preparation of synthesis α-Fe_2O_3: The synthesis of Ferric Oxide (α-Fe_2O_3) nanoparticles with some modifications was based on Bashir et al. (2020) research and showed in Figure 1B. Fe^{3+} solution (0.1M) stirred at 70 ^oC for 60 minutes combines $FeCl_3 \cdot 6H_2O$ and deionized water. 100 ml of PP extract was slowly added to the Fe^{3+} solution and stirred at 70 ^oC for 60 minutes (the solution would change from yellow brown to brown). 50 mL (1 mM) of NaOH was slowly added to the solution every 30 min (the solution would change from brown to turn black). The solution would indicating the formation of colloidal iron oxide nanoparticles.

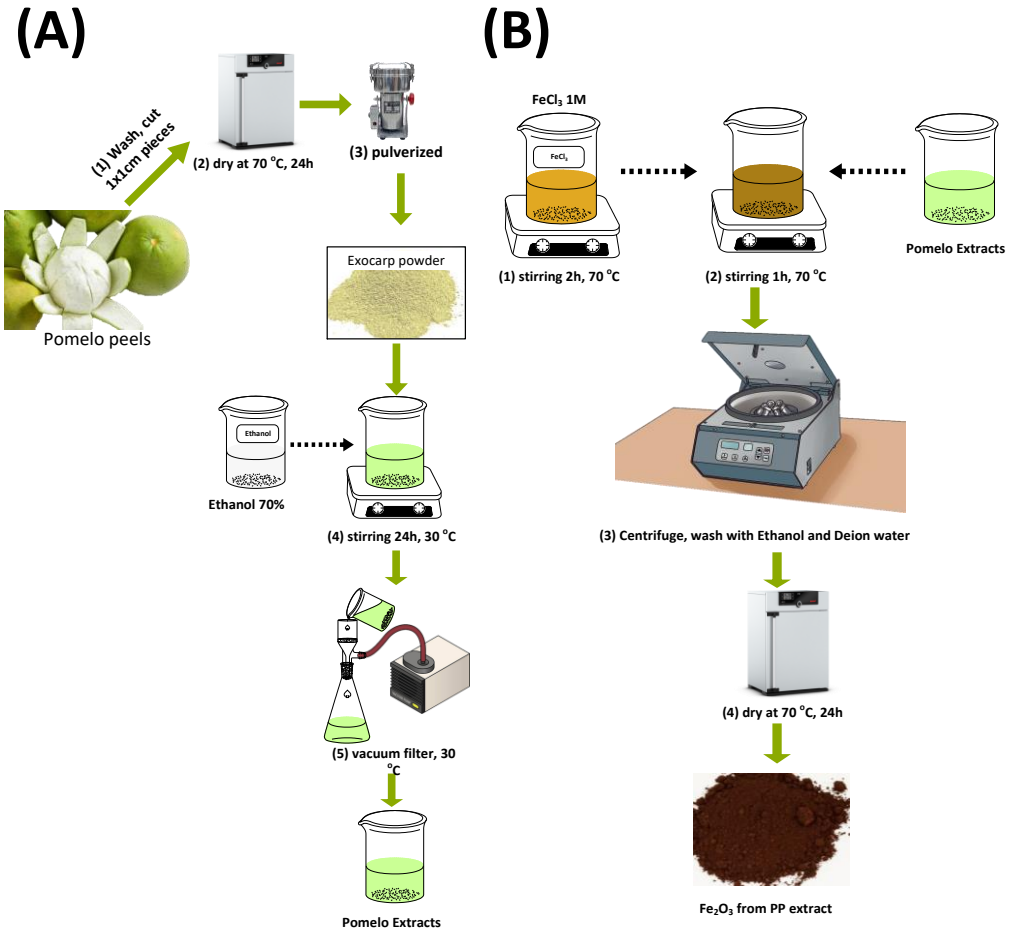

Figure 1. PP extract extraction process (A) and α- Fe_2O_3 synthesis process (B)

Characterization

The surface morphology and element of α-Fe_2O_3 were examined by Energy Dispersive X-ray Spectroscopy (EDX) and Scanning Electron Microscopy (SEM) using Hitachi S-4800 system, Japan. The functional groups of the α-Fe_2O_3 were analyzed in the range of 4000 cm^{-1} - 400 cm^{-1} coated with KBr powder by a Nicolet 6700 Spectrometer (FTIR). Crystallinity and structure were determined via X-ray diffraction at a scan rate of 2°.min^{-1} (2θ) with CuK radiation (1.5406 Å) using a Siemens D5000 diffractometer. The surface area and pore size of α-Fe_2O_3 were analyzed by Static Volumetric Gas Adsorption (SVGA) using N_2 gas adsorption/desorption with 1 g.$(cm^3)^{-1}$ degas at 150 ºC for 12 h and tested in the Micro Active for TriStar II Plus 2.03 (High Throughput Surface Area and Porosity Analyzer). A UV-Vis spectrophotometer (Metash UV-5100 spectrophotometer) was used to analyze dyes concentrations in solution samples.

Adsorption experiment

Adsorption evaluation experiments were performed based on the procedure performed in previous studies with some changes (Lam *et al.*, 2023; Quyen *et al.*, 2023; Van Phuoc *et al.*, 2023). 0.1 gram of Fe_2O_3 nanoparticles and 100 mL of dyes solution (concentration of 50 mg/L, pH6) were added to 250 mL Erlenmeyer. Then, the sample was shaken in Incubator shaker (JEOTECH IST-4075R - Korean) at 30 ºC for 2 hours. The sample mixture was centrifuged 6000 rpm to recover the color solution after adsorption. Adsorption capacity (qe) and adsorption efficiency (H%) were calculated by

applying Formula (1)-(2). In which, the initial dye concentration (C_0) and the equilibrium dye concentration (C_f) were determined by a UV-Vis spectrophotometer.

$$q_e(\text{mg}.g^{-1}) = \frac{(C_0 - C_f)\ (mg.L^{-1})}{\text{Dosage}\ (\text{g}.L^{-1})} \quad (1)$$

$$H\ (\%) = \frac{(C_0 - C_f)\ (mg.L^{-1})}{C_0\ (mg.L^{-1})} \times 100 \quad (2)$$

The acids/bases surface and zeta potential measurement (pHpzc)

The pH point zero charge (pHpzc) was tested by the method reported in Thuan and Bich et al. (2021), Van Tran et al. (2017) study. 0.1gram Fe_2O_3 nanoparticles and 100 mL KCl solution (0.1 mol/L) were added in Erlenmeyer with pH from pH2 to pH10 values (Adjust with KOH and HCl concentrations of 0.1M and 0.01M). The samples were shaken for 3 hours and stabilized for 24 hours at room temperature. The initial pH (pHi) and pH final (pHf) values were recorded by using a Hanna Instruments HI2210-02 bench machine pH meter. pHpzc was determined at crosspoint between pHi and pHf on the pH value chart (Kosmulski, 2020, 2023; https://goldbook.iupac.org/terms/view/P04775).

Washing and reuse process

The material was evaluated at the best condition selected after the evaluation of influencing factors. The material after the initial adsorption process was washed with 3 solvents: water, ethanol and actone to select the appropriate solvent. In which, 1g of material was washed with 100 mL of solvent and the washing process was repeated 4 times to remove all organic dyes. Then the material was dried at 70 ^{0}C for 36 hours to dry completely, when the humidity was below 5%. Next, the material was adsorbed at the initial evaluation conditions. The reuse process stopped when the difference between the initial adsorption capacity and the n^{th} time > 50%.

Adsorption kinetics and isotherm model

The adsorption mechanism helps explain the interaction between α-Fe_2O_3 nanoparticles and dye through prediction from models. Kinetic and isothermal models were executed from the equations in the form of nonlinear models based on Quyen et al. (2023). The model's coefficients with the adjusted coefficient (R^2_{adj}) were calculated based on formulas and presented in Table 1.

Table 1. Equations of kinetic and isothermal models

Model name	Equation	Ref
Adsorption isotherm		
Langmuir	$q_e = \frac{q_m K_L C_e}{1+K_L C_e}$ $(R_L = \frac{1}{1+K_L C_o})$	(Quyen *et al*., 2023)
Freundlich	$q_e = K_F C_e^{1/n}$	(Quyen *et al*., 2023)
Dubinin–Radushkevich (DR)	$q_e = q_m e^{-BE^2}$ $(E=\frac{1}{\sqrt{2B}};\ \varepsilon = R.T.\ln(1+\frac{1}{C_e}))$	(Quyen *et al*., 2023)
Temkin	$q_e = B_T \ln(K_T C_e)$ $(B_T = \frac{RT}{b})$	(Quyen *et al*., 2023)
Adsorption kinetics		
Pseudo–first–order (PFO)	$q_t = q_e(1 - e^{-k_1 t})$	(Quyen *et al*., 2023)
Pseudo–second–order (PSO)	$q_t = \frac{q_e^2 k_2 t}{1 + k_2 t q_e}$	(Quyen *et al*., 2023)
Bangham	$q_t = k_B t^{\alpha_B}$	(Quyen *et al*., 2023)
Evlovich	$q_t = \frac{1}{\beta} ln(1 + \alpha\beta t)$	(Quyen *et al*., 2023)

3. Results and Discussion

Structural Characteristics

The sample was centrifuged to collect solids and washed several times with deionized water and ethanol to remove residual iron and residual extract from the sample. After washing, the sample was dried at 80 ^{0}C for 48 hours and fine crushing to obtain pretreatment Fe_2O_3 powder. Then the Fe_2O_3 powder was calcined in a furnace at 450 ^{o}C for 5 hours, to get the most stable Fe_2O_3 product. The overall reaction mechanism is explained in Equations (3)-(9) based on the research of Bashir et al. (2020):

$$FeCl_3 \rightarrow Fe^{+3} + 3Cl^{-}, \quad (3)$$

$$nFe^{+3} + 3(Ar - OH)_n \rightarrow nFe^0 + 3n(Ar = O) + 3nH^{+}, \quad (4)$$

$$nFe^0 + nH_2O \rightarrow 2Fe^{+2} + 2Fe^{+3} + H_2 + 2OH^{-}, \quad (5)$$

$$nFe^{+3} + nOH^{-} \rightarrow nFe(OH)_3, \quad (6)$$

$$nFe(OH)_3 \rightarrow nFeOOH \downarrow + H_2O, \quad (7)$$

$$nFeOOH \rightarrow nFe_2O_3 + nH_2O, \quad (8)$$

$$2Fe_2O_3 + O_2 \rightarrow 2Fe_2O_3. \quad (9)$$

The morphology of iron oxide nanoparticles mediated by PP extraction was analyzed by scanning electron microscopy (SEM). SEM results are shown in Figure 2 with dimensions of 5 µm and 1 µm. The iron oxide particles have a heterogeneous cubic shape due to the interaction of phytochemical compounds contained in the PP extract with the precursor material. The SEM image clearly shows the morphology of Fe_2O_3 at a much larger size, consistent with the results in Sayed Farheen's study. The $FeCl_3$ precursor used to synthesize Fe_2O_3 will have the form Fe_2O_3 with a cubic shape at the size of 120nm (Sayed & Polshettiwar, 2015). This shows that Fe_2O_3 material using PP extract has been successfully synthesized.

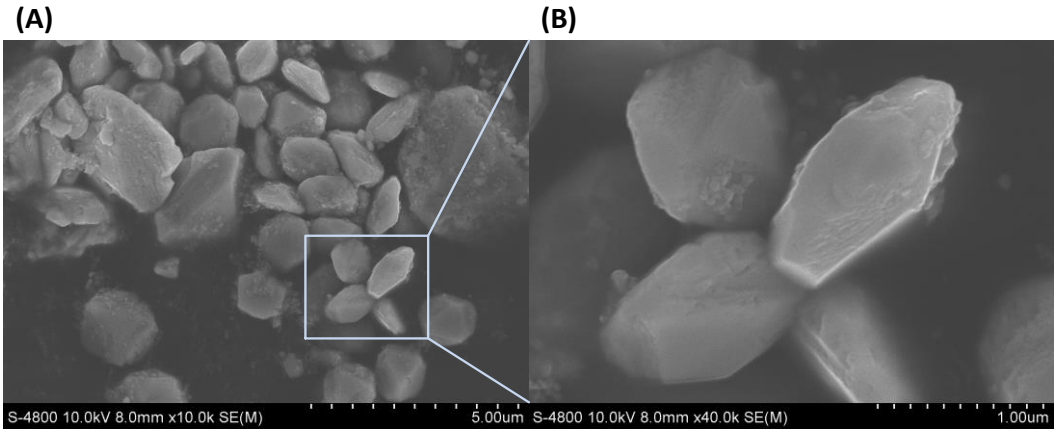

Figure 2. SEM image of Fe_2O_3 at size 5 µm (A) and 1 µm (B)

Crystal structure of Fe_2O_3 material from PP extract was determined by XRD and EDX methods and shown in Figure 3. The XRD spectrum clearly shows the crystalline phases of Fe_2O_3, in which 2θ = 24.19° (012), 33.19° (104), 35.68° (101), 40.91° (113), 49.49° (024), 54.09° (116), 57.66° (122), 62.47° (214), 64.04° (300). The observed narrow and intense peaks can identify the well-crystalline structure of α-Fe_2O_3 of green chemical synthesis (Ali *et al*., 2017). The diffraction peaks show the hexagonal crystal

characteristics of α-Fe_2O_3 and were similarly demonstrated in the research of Hang and Anh (2021), Sayed and Polshettiwar (2015). The crystal size calculated using Debye Scherrer's formula is 72.16 nm (Fatimah *et al.*, 2021). EDX spectroscopy was used to study the elemental composition of nanoparticles. The results show that the detected elements include Fe (iron), O (oxygen) and C (carbon). In which the mass ratio of Iron and Oxygen in the samples is 50.96% and 35.56% respectively, in addition carbon is 13.48%. The carbon content existing in the sample is believed to be from the extract left over during the synthesis process. The presence of these bioactive derivatives can act as a reducing agent, which is a necessary step in the synthesis of the material (Sithara *et al.*, 2024). It can be seen that the production of iron oxide nanoparticles using PP extract has potential.

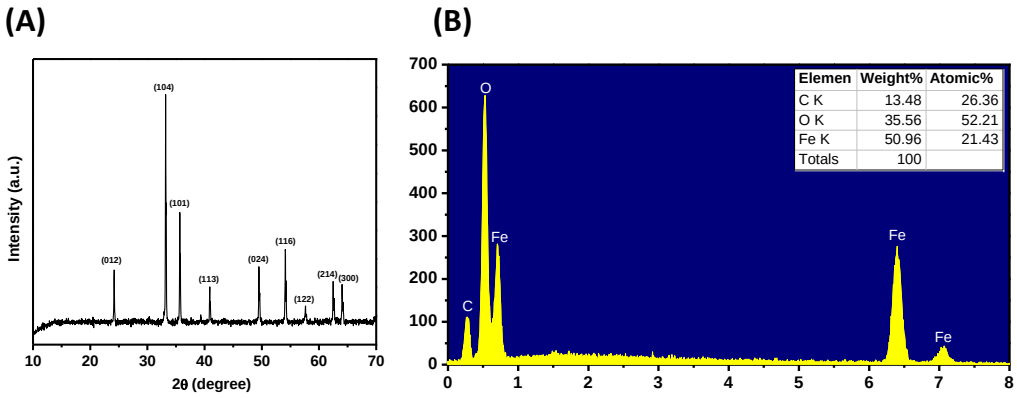

Figure 3. XRD (A) and EDX (B) Spectrum of Fe_2O_3

Infrared spectroscopy (FTIR) analysis method was used to identify functional groups on the surface of α-Fe_2O_3 particles from PP extract, the results of FTIR spectroscopy are shown in Figure 4A. FTIR analysis of the nanoparticles revealed the presence of several characteristic bands. The peak at 3411 cm^{-1} characterizes the stretching vibration of the O–H group. The peak at 1631 cm^{-1} represents the bending vibration of the OH group. This functional group OH is thought to be due to water adsorbed in the sample during synthesis (Ali *et al.*, 2017; Ramesh *et al.*, 2019). The peaks at 546 cm^{-1} and 470 cm^{-1} are attributed to the existence of the metallic oxygen (Fe–O) band (Richard & Ronal, 1971). In Ramesh et al. (2019) study, the formation of Fe-O nanoparticles was similarly confirmed from the strong absorption peaks. In Saeid Taghavi Fardood's study the stretching at the 546 cm^{-1} peak corresponds to the knife intrinsic stretching action of Fe↔O. For the 470 cm^{-1} peak is assigned to the bending vibration of, O↔Fe↔O (Taghavi *et al.*, 2017). The results of N_2 adsorption and desorption are shown in Figure 4(B), indicating the surface area of the material and the formation of pores when α-Fe_2O_3 molecules are stacked on top of each other. BET analysis results show that α-Fe_2O_3 has a specific surface area of 2.68 m^2/g and a pore size of 13.91 nm. N_2 the isotherm of the material at a very small pressure difference shows that the material has a rough, flat, non-porous surface. The characteristics of the adsorption isotherm show that the material tends to follow a second-order isotherm with the mechanism of gas molecules dispersing into the pores on the α-Fe_2O_3 surface, creating an adsorption force with chemical bonding of the α-Fe_2O_3 surface. The adsorption process is described by adsorption constants and energy parameters of the adsorption process such as maximum

adsorption energy and activation energy of the adsorption process, according to the standard classification of isotonic curves in IUPAC adsorption heat.

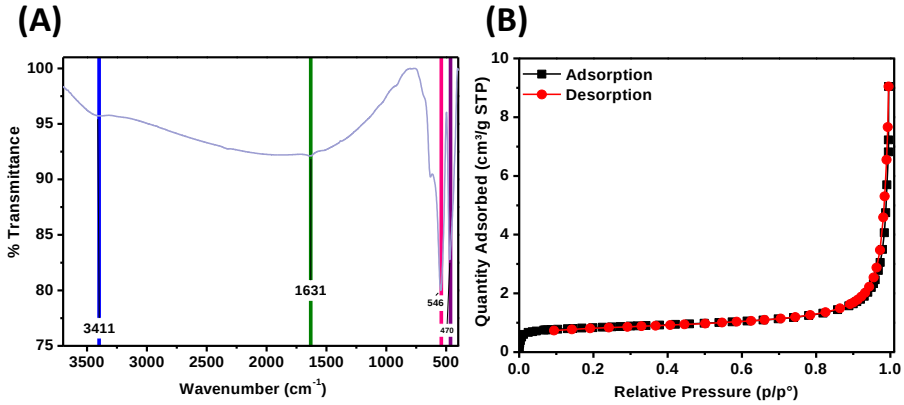

Figure 4. FTIR diagram (A) and N_2 adsorption-desorption isotherm (B) of Fe_2O_3

Selective adsorption evaluation

The selective adsorption ability was evaluated on 4 dyes of the cation group (Methylene Blue (MB), Brilliant Green (BG)) and anion group (Congo Red (CR), Methyl Red (MR)). Selective evaluation results were shown in Figure 5, the material had better adsorbent than the anion group and the cation group. In the anion dyes group, α-Fe_2O_3 was the best adsorbent with CR with an adsorbent capacity of 13 mg/g. In the Canion group, α-Fe_2O_3 was the best adsorbent with BG with an adsorbent capacity of 10 mg/g. Two pigments (BG and CR) were selected to predict the adsorbent mechanism of α-Fe_2O_3 materials.

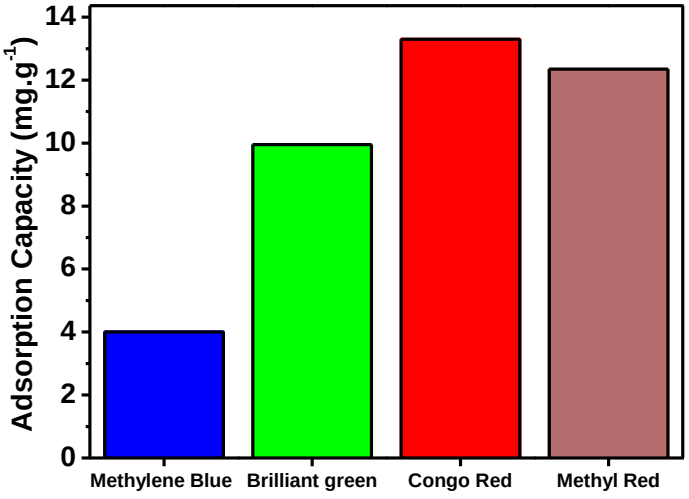

Figure 5. Evaluate the adsorption capacity of MB, BG, CR and MR

Evaluation of influential factors

The effect results of the α-Fe_2O_3 dosage on the adsorption capacity were presented in Figure 6. With BG, the adsorption efficiency was increased rapidly from 25% to 68% when the α-Fe_2O_3 dosage increased from 0.5 g/L to 3 g/L. The dosage increases from 3

g/L to 4 g/L, but the adsorption capacity as well as the adsorption efficiency both decreases. This was thought to be the α-Fe_2O_3 dosage due to excessive use and hindering the adsorption process. With CR, the treatment efficiency was increased rapidly from 18% to 53% when the α-Fe_2O_3 dosage increased from 0.5 g/L to 1 g/L. When the concentration was increased from 1 g/L to 4 g/L, the efficiency increased steadily from 55% to 100%. The results showed that the maximum adsorbent material was at the dosage of 3 g/L with BG and 4 g/L with CR. Therefore, dosages of 3 g/L and 4 g/L were selected to evaluate the next factor.

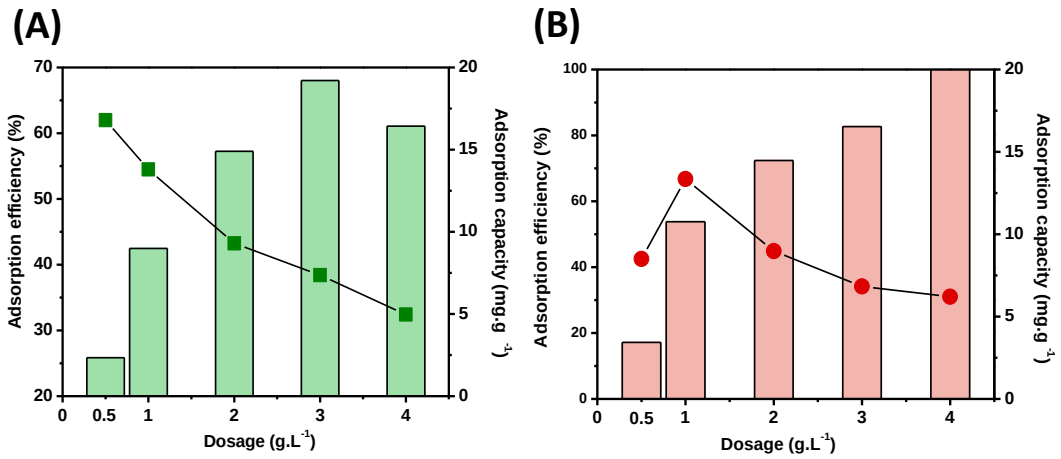

Figure 6. The effects of dosage on the adsorption capacity BG (A) and CR (B)

Temperature was one of the factors that affected the adsorption process. When the temperature increases, the molecules in the solution were also disturbed. Therefore, the temperature factor was evaluated at different temperature ranges (30 ^oC, 40 ^oC, 50 ^oC, 60 ^oC). The adsorption results were shown in Figure 7A with corresponding values for each temperature range. The adsorption process recorded that the adsorption capacity did not change much at different temperature ranges. The highest adsorption capacity of CR color is 20 mg/g at 50 ^oC and BG is 8 mg/g at 30 ^oC and 50 ^oC. From the results it can be seen that the α-Fe_2O_3 material from PP extract is little affected by environmental temperature. Therefore, the temperature value of 50 ^oC was chosen to evaluate the next factors due to the highest adsorption capacity in the temperature ranges. The pH of the solution can affect the adsorption process through affecting surface complexation reactions and electrostatic interactions between CR, BG and α-Fe_2O_3 surface. According to Figure 7B, the solution pH of BG dye gives the highest adsorption capacity at pH4 (5 mg/g). The solution pH of CR colorant gives the highest adsorption capacity at pH8 (20 mg/g). In particular, the adsorption capacity at pH points>6 (favoring basic environment) tends to be higher than the adsorption capacity at pH points<6 (favoring acidic environment). This shows that the material works well in basic environments. In Satheesh's research, α-Fe_2O_3 material also showed good adsorption capacity in basic environments. This is explained by the increase in H^+ ion concentration in the solution which may have promoted the accumulation of H^+ ions on the α-Fe_2O_3 surface when α-Fe_2O_3 adsorbed at low pH. This increase in protonation causes a strong repulsive force between the H^+ ions on the α-Fe_2O_3 surface and the protonated CR. Therefore, CR removal is inhibited at lower pH values. On the contrary, at alkaline pH, excess OH^- ions can accumulate on the α-Fe_2O_3 surface,

causing the electrostatic repulsion between the negative charge on the adsorbent surface and the anionic CR molecule to increase (Satheesh *et al*., 2016). This shows that the capacity. The adsorption amount of CR increased while that of BG decreased. Therefore, pH8 for CR and pH4 for BG were selected as the best pH values to evaluate the next factors.

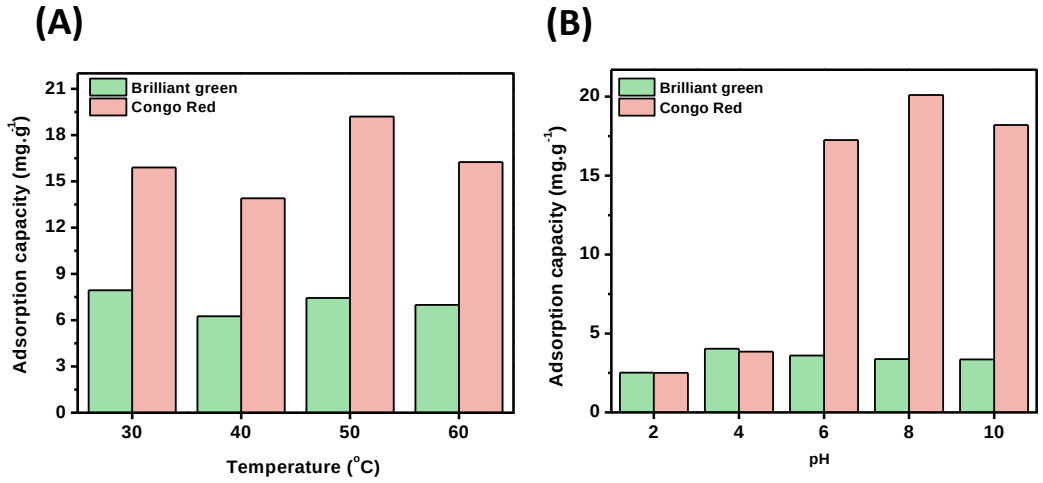

Figure 7. The effects of temperature (A) and pH (B)

The effect of time on the adsorption capacity of α-Fe_2O_3 to CR and BG was conducted with time intervals from 0 to 240 minutes. According to the results in Figure 8A, the adsorption capacity of α-Fe_2O_3 with CR dye increased from 0 to 22 mg/g in the first time period from 0 minutes to 30 minutes. Time from 30 minutes to 120 minutes shows that the adsorption capacity ranges from 22 mg/g to 25 mg/g, time from 120 minutes to 210 minutes, the adsorption capacity begins to decrease from 23 mg/g to 18 mg/g. mg/g. It can be said that the adsorption process has reached an equilibrium state between 30 and 120 minutes. The highest CR color adsorption capacity was recorded at the 60 minute time point of 24.7 mg/g. For BG dye, the adsorption capacity increased from 0 to 5 mg/g in the first time period from 0 minutes to 30 minutes. The time from 30 minutes to 240 minutes shows that the adsorption capacity is in the range of 5 ± 1 mg/g. It can be said that the adsorption process has reached an equilibrium state starting from the 30 minute time point. Therefore, the adsorption time was chosen as the optimal value for the next experiments with CR dye being 60 minutes and BG being 30 minutes.

The results of the investigation of the influence of the concentration of CR and BG dye solutions on the adsorption capacity of α-Fe_2O_3 are presented in Figure 8B. The concentration of CR dye solution was evaluated from 10 mg/L to 300 mg/L. In the concentration range from 10 mg/L to 100 mg/L, the adsorption capacity increased from 8.7 mg/g to 85 mg/g. The adsorption process still increased gradually when the concentration increased to 250 mg/L. When the concentration reached 300 mg/L, the adsorption capacity decreased slightly. It can be seen that the CR adsorption process reached equilibrium at a concentration of 250 mg/L. For BG dye, the adsorption capacity increased from 4.5 mg/g to 24 mg/g in the concentration range from 10 mg/L to 100 mg/L. The adsorption process reached equilibrium when the concentration increased from 100 mg/L to 200 mg/L. When the concentration reached 300 mg/L, the adsorption capacity gradually decreased. It can be seen that the BG adsorption process reached equilibrium at a concentration of 100 mg/L. Therefore, the values chosen were 100 mg/L for BG color

and 250 mg/g for CR color. In summary, the best adsorption capacity of Fe_2O_3 was recorded with CR colorant: time 60 min, temperature 50 ℃, pH8, concentration 1 g/L, concentration 250 mg/L. The best adsorption capacity of Fe_2O_3 was recorded with BG colorant: time 30 min, temperature 30 ℃, pH4, concentration 3 g/L, concentration 100 mg/L. This is the best adsorption condition selected to predict the adsorption mechanism based on mathematical models.

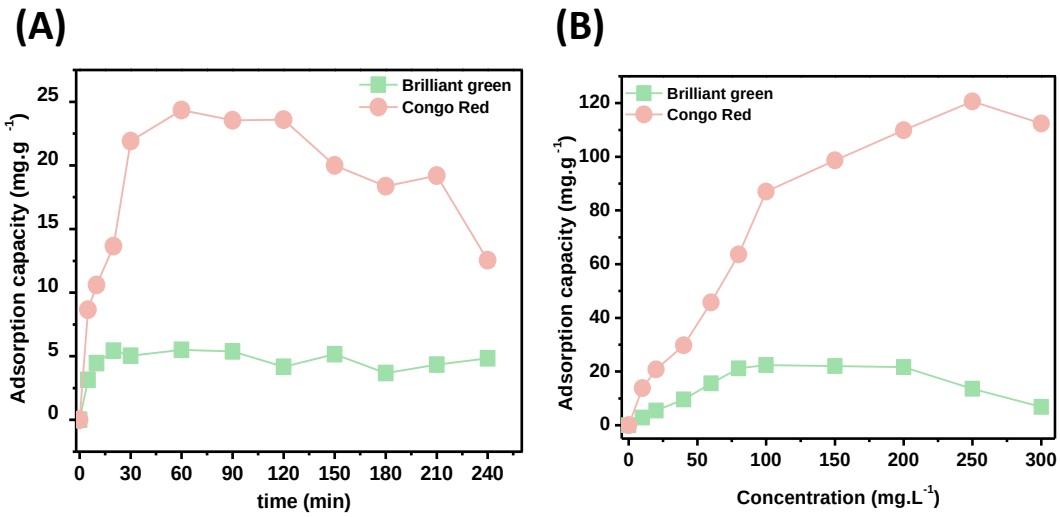

Figure 8. The effects of time (A) and concentration (B)

Evaluation of the kinetic model

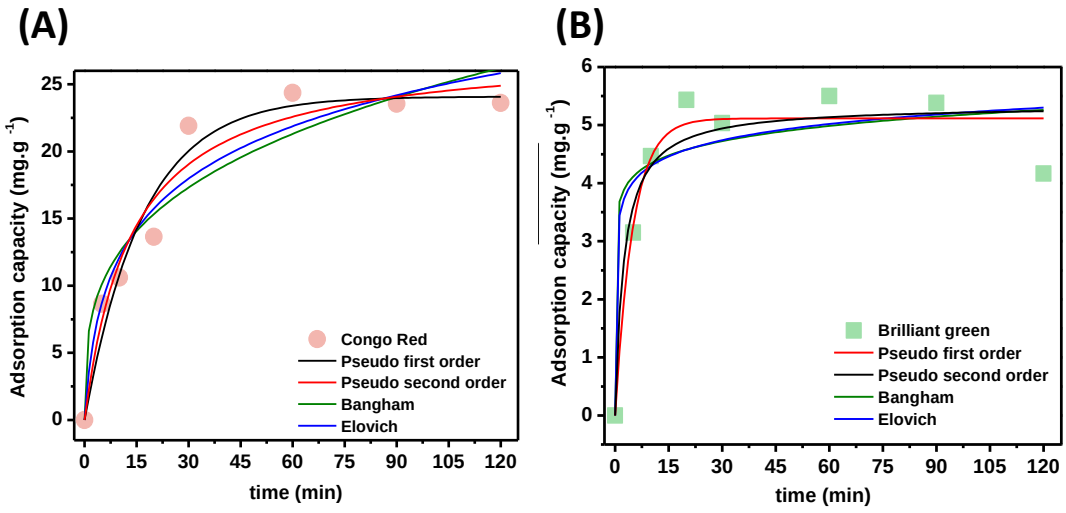

Figure 9. Adsorption kinetics of α-Fe_2O_3 with CR dye (A) and BG dye (B)

The adsorption kinetic model was used to predict the adsorption process of α-Fe_2O_3. The parameters obtained from the adsorption kinetic model of α-Fe_2O_3 with CR and BG pigments have been summarized in Table 2. The diagrams for the first-order pseudo-adsorption kinetics, second-order pseudo-adsorption kinetics, Elovich kinetics and Bangham kinetic models are presented in Figure 9. Table 2 shows that the R^2_{adj} of the

four kinetic models has values in the following order: first-order pseudo-equation (0.958) < second-order pseudo-equation (0.951) < Elovich (0.931)) < Bangham (0.905), which corresponds to the order of compatibility of the models with the experimental data. The PSO and PFO kinetic models are suitable for the adsorption process of the material with high correlation coefficients of R^2_{adj} = 0.955 and 0.95, respectively. In addition, the error functions (χ2, MRE, SSE) of the PSO model are the lowest at 2.205 - 10.471. The results show that the adsorption of CR on α-Fe_2O_3 is mainly controlled by the chemical interaction process on the material surface. Besides, the rate constant k_2 = 0.03 shows that the rate occurs very quickly with the formation of chemical interactions. For BG pigment, the R^2_{adj} of the four kinetic models has the following values in the following order: first-order pseudo-equation (0.937) < second-order pseudo-equation (0.903) < Elovich (0.847) < Bangham (0.841), which corresponds to the order of the compatibility of the models with the experimental data. The PSO and PFO kinetic models are suitable for the adsorption process with R^2_{adj} = 0.937 and 0.903, respectively. In addition, the error functions (χ2, MRE, SSE) of the PFO model are the lowest at 0.217 - 6.790. The results show that the adsorption of BG on α-Fe_2O_3 is mainly controlled by the physical interaction process on the material surface. Besides, the rate constants k_2 = 0.076 and k_1 = 0.202 show that the speed occurs very quickly. Although the adsorption rate by chemical interactions is faster than by physical interactions, BG is largely adsorbed thanks to physical interactions. Proving that the adsorption of CR and BG on α-Fe_2O_3 is controlled by physical and chemical interaction mechanisms on the material surface. However, the physical interaction mechanism largely accounts for controlling the adsorption process of CR and BG on α-Fe_2O_3.

Table 2. Parameters for adsorption of Fe_2O_3 from PP extract

Name model	Parameter	CR	BG
PFO	q_e (mg/g)	24.077	5.115
	k_1 (min^{-1})	0.060	0.202
	R^2_{adj}	0.958	0.937
	Chi-square (χ2)	2.407	0.217
	MRE	9.865	6.790
	SSE	20.442	1.303
PSO	q_e (mg/g)	27.726	5.347
	k_2 (min^{-1})	0.003	0.076
	R^2_{adj}	0.951	0.903
	Chi-square (χ2)	2.205	0.332
	MRE	10.471	9.653
	SSE	2.893	1.994
Elovich	β (g⁄mg)	0.172	2.477
	α (mg/(g.min))	4.080	1692.387
	R^2_{adj}	0.931	0.847
	Chi-square (χ2)	5.597	0.526
	MRE	10.131	13.222
	SSE	33.580	3.155
Bangham	k_B (mL/(g/L))	6.260	3.627
	α_B	0.299	0.078
	R^2_{adj}	0.905	0.841
	Chi-square (χ2)	7.650	0.548
	MRE	13.382	13.612
	SSE	45.897	3.286

Evaluation of the isothermal model

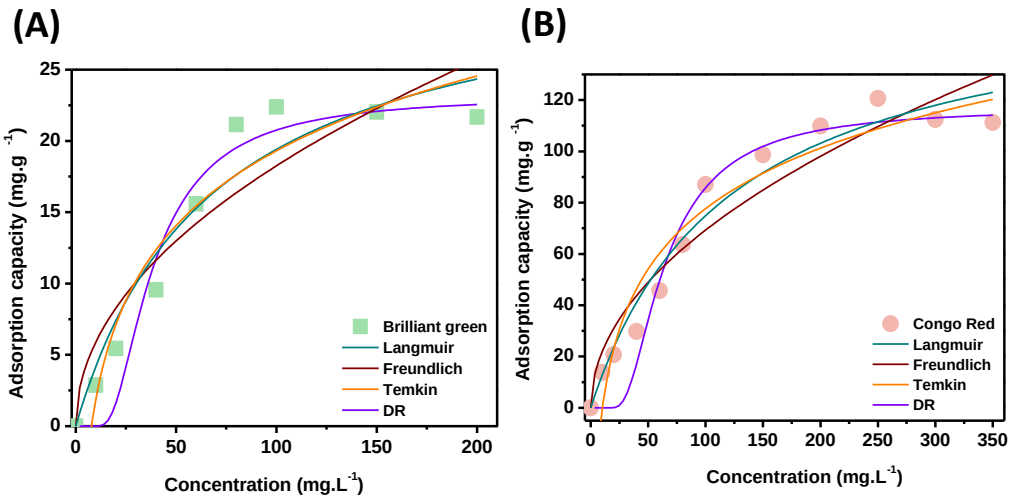

Figure 10. Adsorption isotherm of Fe_2O_3 with BG dye (A) and CR dye (B)

The adsorption isotherm model is used to determine the adsorption capacity and explain the mechanism of the combination of color molecules into the adsorbent and the relative affinity of the color molecules to the adsorbent. The Langmuir, Freundlich, Temkin and D – R adsorption isotherm models are presented in Figure 10. The parameters obtained from the adsorption isotherm model of α-Fe_2O_3 with CR and BG pigments are summarized in Table 3. For CR color, the fit of the experimental data with the models isotherm is determined by its corrected R^2_{adj} in the following order: Langmuir (0.964) > DR (0.952) > Temkin (0.943) > Freundlich (0.874). Furthermore, the error functions (χ2, MRE and SSE) of the isotherm models also confirm that the Langmuir isotherm has the lowest error function values so it is a good model fit. best for CR adsorption onto α-Fe_2O_3. In addition, the maximum adsorption capacity recorded from the model is 130.700 mg/g.

For BG color, the fit of the experimental data with the models isotherm is determined by its corrected R^2_{adj} in the following order: DR (0.962) > Langmuir (0.912) > Temkin (0.906) > Freundlich (0.837). Furthermore, the error functions (χ2, MRE and SSE) of the isotherm models also confirm that the Langmuir isotherm has the lowest error function values so it is a good model fit. best for BG adsorption onto α-Fe_2O_3. In addition, the maximum adsorption capacity recorded from the model is 33.701 mg/g. It can be seen that the Langmuir isotherm model appropriately describes the adsorption process of CR and BG on α-Fe_2O_3 corresponding to the $R^2_{adj} \geq 0.90$. The results show that α-Fe_2O_3 is a monolayer material, interactions occur on the surface. The results show that the α-Fe_2O_3 adsorption process is a monolayer adsorption, physical and chemical interactions occurring on the α-Fe_2O_3 surface play an important role in the adsorption process of CR and BG. In Saima Noreen's research, similar results were obtained when the α-Fe_2O_3 material showed a high correlation coefficient with the Langmuir model when adsorbing CR dye. This shows that the characteristics of α-Fe_2O_3 materials when synthesized from natural extracts will have nearly the same adsorption tendency (Noreen *et al*., 2020).

Table 3. Isothermal parameters for the adsorption of Fe_2O_3 from PP extract

Name model	Parameter	CR	BG
Langmuir	K_L (L/mg)	0.058	0.046
	q_m (mg/g)	130.700	33.701
	R^2_{adj}	0.964	0.912
	Chi-square ($\chi 2$)	70.099	8.454
	MRE	13.669	20.957
	SSE	700.991	76.082
	R_L	0.428	0.438
Freundlich	K_F (mg/g)	22.456	4.222
	1/n (min^{-1})	0.336	0.426
	R^2_{adj}	0.874	0.837
	Chi-square ($\chi 2$)	245.727	15.595
	MRE	33.352	30.371
	SSE	2457.266	140.349
Temkin	B_T	26.695	8.262
	k_T (L/mg)	0.609	0.336
	R^2_{adj}	0.943	0.906
	Chi-square ($\chi 2$)	112.214	8.961
	MRE	92.420	86.892
	SSE	69605.991	3432.196
D - R	B (mol^2/kJ^2)	17.767	23.418
	q_m (mg/g)	111.303	25.985
	E (kJ/mol)	0.168	0.146
	R^2_{adj}	0.952	0.962
	Chi-square ($\chi 2$)	93.656	3.624
	MRE	96.149	99.998
	SSE	67128.987	4128.807

Reusability assessment

The materials after the adsorption evaluation process were evaluated for reusability in order to improve their applicability. The materials were adsorbed under the best conditions for CR (time 60 min, temperature 50 ℃, pH8, concentration 1 g/L, concentration 250 mg/L) and BG (time 30 min, temperature 30 ℃, pH4, concentration 3 g/L, concentration 100 mg/L). Then, the material was washed with different solvents and reused. The results of the evaluation of the washing and reused solvents are shown in Figure 11. It can be observed that water and ethanol are the two most effective solvents for removing BG and CR from the material. The washing process was repeated many times to remove them completely. In which water is the best solvent for CR, with an adsorption capacity of 65.45 mg/g of material after washing. Ethanol is the best solvent for BG, with an adsorption capacity of 18 mg/g of material after washing. In addition, the reuse process was performed three times, with the adsorption capacity reduced by more than 90% compared to the initial one. The results showed that the initial adsorption capacity was 122 mg/g for CR and 26 mg/g for BG. After the first reuse, the adsorption capacity decreased to 65 mg/g for CR and 18 mg/g for BG, corresponding to a decrease of 31% to 47%. In the second reuse, the adsorption capacity was 9.3 mg/g for BG and 18.7 mg/g, corresponding to a decrease of 64% to 84%. The third reuse showed that the material had almost lost its adsorption capacity. The results showed that the material could only be reused once. This shows that the material after the adsorption process is very difficult to wash and remove the dyes again. This is a point that needs to be studied

to develop and improve the adsorption and reuse capacity of the material or apply the adsorbed material for the next treatment process.

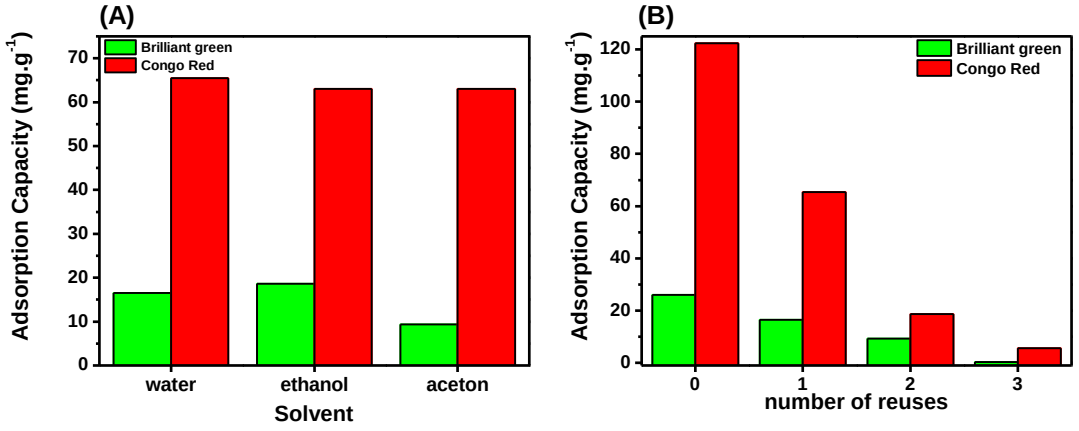

Figure 11. Effect of washing solvent and reusability of material

Comparison with other studies

Table 4. Comparison with other studies.

Sample	extract	pollutant	Adsorption capacity (mg/g)	ref
rGO/γ- Fe_2O_3		Malachite green	64.26	(Zhu *et al*., 2025)
Fe_2O_3- basalt		As(III)	5.39	(Song *et al*., 2025)
Fe_2O_3- basalt		As(V)	5.71	(Song *et al*., 2025)
pectin/ Fe_2O_3		Brilliant green	27.79	(Hien *et al*., 2025)
pectin/ Fe_2O_3		Crystal violet	23.43	(Hien *et al*., 2025)
Fe_2O_3		Congo red	104.17	(Borth *et al*., 2021)
Fe_3O_4		Titan yellow	30	(Pietrzyk *et al*., 2022)
graphene-iron		Congo red	31.71	(Ahmed *et al*., 2023)
ϒ- Fe_2O_3	orange peel	Congo red	1417.7	(Hoang *et al*., 2024)
Fe_2O_3	microalgae	Crystal violet	256.4	(Shalaby *et al*., 2021)
Fe_2O_3	microalgae	Methyl orange	270.2	(Shalaby *et al*., 2021)
α-Fe_2O_3	cactus cladode	Methylene blue	358.48	(Abdedayem *et al*., 2025)
Fe_2O_3	Acacia jacquemontii	Brilliant green	60	(Choudhary *et al*., 2025)
Fe_2O_3	*Piper haba* steam	Congo red	88	(Yesmin *et al*., 2024)
Fe2O3-Ag	guajava leaves	Cr(VI)	71.34	(Biswal *et al*., 2020)
Fe_2O_3	Microalgal	Crystal violet	55.62	(Bhukal *et al*., 2022)
α-Fe_2O_3	Pomelo peel	Congo red	130.70	This work
α-Fe_2O_3	Pomelo peel	Brilliant green	33.70	This work

To have an objective assessment of the material, comparison with other studies has been discussed and shown in Table 4. The results show that Fe_2O_3 synthesised by the chemical method had a low adsorption capacity. In which Congo red had the highest adsorption capacity of 104.17 mg/g. Next was Malachite green with an adsorption capacity of 64.26 mg/g. For other dyes, the adsorption capacity was only about 20-30

mg/g. The adsorption capacity of metal ions was very low, with almost no adsorption capacity. In addition, Fe_2O_3 synthesised by the green chemistry method (using extraction) has significantly improved adsorption capacity. The results show that for the dye Congo red, the adsorption capacity was recorded from 88 to 1417 mg/g. For other dyes, the adsorption capacity was recorded from 33 to 350 mg/g. It could be seen that, depending on the type of extract, the adsorption capacity was also different. In which Fe_2O_3 with the α-Fe_2O_3 structure has lower adsorption than the ϒ- Fe_2O_3 structure. Overall, it can be seen that the green synthesis method is both environmentally friendly and has good adsorption capacity. This is a bright spot for further research.

4. Conclusion

In this study, α-Fe_2O_3 materials were synthesized by the new green chemical method of PP extract. Through the methods of analyzing SEM, FTIR, XRD and BET methods, it shows that the object had a heterogeneous shape. Materials were identified and iron oxygen by identifying iron and oxygen elements with a ratio of 50.96% and 35.56%. Along with vertices 2θ = 24.19 ° (012), 33.19 ° (104), 35.68 ° (101), 40.91 ° (113), 49.49 ° (024), 54.09 ° (116), 57.66 ° (122), 62.47 ° (214), 64.04 ° (300). The crystal size was calculated by the Debye Scherrer's formula of 72.16 nm. The vertices at 546 cm^{-1} and 470 cm^{-1} were given the existence of metal oxygen bands (M - O) clearly defined. In addition, OH groups were thought to be the presence of the extract of the PP skin. Best adsorption conditions of α-Fe_2O_3 were recorded with CR: 60 minutes, temperature 50 ℃, pH8, dosage 1 g/L, concentration of 250 mg/L. best adsorption conditions of Fe_2O_3 were recorded with BG: 30 minutes, temperature 30 ℃, pH4, dosage 3 g/L, concentration of 100 mg/L. This was the best adsorption condition to predict the adsorption mechanism based on mathematical models. The adsorption process was consistent with the PSO and PFO kinetic models, which are mainly controlled by physical and chemical interactions on the surface. Lamguir adsorption isotherm with monolayer adsorption mechanism, occurring on α-Fe_2O_3 surface. This was a point that requires further in-depth research. In summary, Fe_2O_3 from green chemistry was a potential material to replace materials synthesized from conventional chemical methods. It has good adsorption capacity which reduces production costs and disposal problems.

Acknowledgement

The author acknowledges the Nguyen Tat Thanh University for supporting this work. This research was fund by a grant from the Science and Technology Development Foundation of Nguyen Tat Thanh University with code (2024.01.11/HĐ-KHCN).

References

Abbas, Z.M.A., Shatti, W.A., Mohammad, A.M. & Khodair, Z.T. (2024). Magnetic iron oxide: Preparation and characterization for antibacterial activity applications. *Journal of Sol-Gel Science and Technology*, *109*(2), 534-542. https://doi.org/10.1007/s10971-023-06300-w

Abdedayem, A., Chemingui, H., Nouri, H., Hafiane, A. & Ben Amor, T. (2025). Green iron oxide nanoparticles from Opuntia ficus-indica (L.) extract for efficient dye removal: Optimization and mechanism investigation. *Biomass Conversion and Biorefinery*, 15, 20817-20838. https://doi.org/10.1007/s13399-025-06656-9

Abdullah, J.A.A., Salah Eddine, L., Abderrhmane, B., Alonso-González, M., Guerrero, A. & Romero, A. (2020). Green synthesis and characterization of iron oxide nanoparticles by

pheonix dactylifera leaf extract and evaluation of their antioxidant activity. *Sustainable Chemistry and Pharmacy*, 17. https://doi.org/10.1016/j.scp.2020.100280

Ahmed, D.N., Hussein, M.A., Abdul-Kareem, M.B., Hassan, W.H., Al-Ansari, N. & Faisal, A.A.H. (2023). Green synthesis of hybrid iron oxides/graphene immobilization on the iron slag for reclamation Congo red dye-water. *Water, Air & Soil Pollution, 234*(12), 778. https://doi.org/10.1007/s11270-023-06806-7

Ali, H.R., Nassar, H.N. & El-Gendy, N.S. (2017). Green synthesis of α-Fe_2O_3 using citrus reticulum peels extract and water decontamination from different organic pollutants. *Energy Sources, Part A: Recovery, Utilization and Environmental Effects, 39*(13), 1425-1434. https://doi.org/10.1080/15567036.2017.1336818

Bashir, M., Ali, S. & Farrukh, M.A. (2020). Green synthesis of Fe_2O_3 nanoparticles from orange peel extract and a study of its antibacterial activity. *Journal of the Korean Physical Society, 76*(9), 848-854. https://doi.org/10.3938/jkps.76.848

Bhukal, S., Sharma, A., Rishi, Divya, Kumar, S., Deepak, B., Pal, K. & Mona, S. (2022). Spirulina based iron oxide nanoparticles for adsorptive removal of crystal violet dye. *Topics in Catalysis, 65*(19-20), 1675-1685. https://doi.org/10.1007/s11244-022-01640-3

Bich, N.H., Thuong, T.N., Dai, V.N. & Lam, V.T. (2021). Removal of crystal violet from aqueous solution using environment-friendly and water-resistance membrane based on polyvinyl/agar/maltodextrin. *Materials Today: Proceedings*, 38, 3046-3052. https://doi.org/10.1016/j.matpr.2020.09.391

Biswal, S.K., Panigrahi, G.K. & Sahoo, S.K. (2020). Green synthesis of Fe_2O_3-Ag nanocomposite using psidium guajava leaf extract: An eco-friendly and recyclable adsorbent for remediation of Cr(VI) from aqueous media. *Biophysical Chemistry*, 263, 106392. https://doi.org/10.1016/j.bpc.2020.106392

Borth, K.W., Galdino, C.W., Teixeira, V. de C. & Anaissi, F.J. (2021). Iron oxide nanoparticles obtained from steel waste recycling as a green alternative for Congo red dye fast adsorption. *Applied Surface Science*, 546, 149126. https://doi.org/10.1016/j.apsusc.2021.149126

Bouafia, A., Laouini, S.E., Khelef, A., Tedjani, M.L. & Guemari, F. (2021). Effect of ferric chloride concentration on the type of magnetite (Fe_3O_4) nanoparticles biosynthesized by aqueous leaves extract of Artemisia and assessment of their antioxidant activities. *Journal of Cluster Science, 32*(4), 1033-1041. https://doi.org/10.1007/s10876-020-01868-7

Chiavola, A. (2011). Textiles. *Water Environment Research, 83*(10), 1532-1548. https://doi.org/10.2175/106143011X13075599869812

Choudhary, N., Patel, B., Desai, R., Dawane, V., Luhana, K., Vyas, S., … & Patel, A. (2025). Adsorption of brilliant green dye by iron oxide nanoparticles synthesized from the leaf extracts of acacia jacquemontii. *IEEE Transactions on NanoBioscience, 24*(2), 234-248. https://doi.org/10.1109/TNB.2025.3528131

Clarke, C.J., Tu, W.C., Levers, O., Bröhl, A. & Hallett, J.P. (2018). Green and sustainable solvents in chemical processes. *Chemical Reviews, 118*(2), 747-800. https://doi.org/10.1021/acs.chemrev.7b00571

Debnath, A., Deb, K., Das, N.S., Chattopadhyay, K.K. & Saha, B. (2016). Simple chemical route synthesis of Fe_2O_3 nanoparticles and its application for adsorptive removal of Congo red from aqueous media: Artificial neural network modeling. *Journal of Dispersion Science and Technology, 37*(6), 775-785. https://doi.org/10.1080/01932691.2015.1062772

Dehbi, A., Dehmani, Y., Omari, H., Lammini, A., Elazhari, K., Abouarnadasse, S. & Abdallaoui, A. (2020). Comparative study of malachite green and phenol adsorption on synthetic hematite iron oxide nanoparticles (α-Fe_2O_3). *Surfaces and Interfaces*, 21, 100637. https://doi.org/10.1016/j.surfin.2020.100637

Eldeeb, B.A., El-Raheem, W.M.A. & Elbeltagi, S. (2023). Green synthesis of biocompatible Fe_3O_4 magnetic nanoparticles using citrus sinensis peels extract for their biological activities and magnetic-hyperthermia applications. *Scientific Reports, 13*(1). https://doi.org/10.1038/s41598-023-46287-6

Fatimah, S., Ragadhita, R., Al Husaeni, D.F. & Nandiyanto, A.B.D. (2021). How to calculate crystallite size from x-ray diffraction (XRD) using Scherrer method. *ASEAN Journal of Science and Engineering*, *2*(1), 65-76. https://doi.org/10.17509/ajse.v2i1.37647

Fernández, C., Larrechi, M.S. & Callao, M.P. (2010). An analytical overview of processes for removing organic dyes from wastewater effluents. *TrAC Trends in Analytical Chemistry, 29*(10), 1202-1211. https://doi.org/10.1016/j.trac.2010.07.011

Gómez-López, P., Puente-Santiago, A., Castro-Beltrán, A., Santos do Nascimento, L.A., Balu, A.M., Luque, R. & Alvarado-Beltrán, C.G. (2020). Nanomaterials and catalysis for green chemistry. *Current Opinion in Green and Sustainable Chemistry*, 24, 48-55. https://doi.org/10.1016/j.cogsc.2020.03.001

Hang, B.T., Anh, T.T. (2021). Controlled synthesis of various Fe_2O_3 morphologies as energy storage materials. *Scientific Reports, 11*(1), 5185. https://doi.org/10.1038/s41598-021-84755-z

Hien, T.T., Hoang, B.N., Nguyen, L.M., Hoang, A.M., Doan, Q.M.T. & Bach, L.G. (2025). Synthesis of pectin/Fe_2O_3 membrane from pomelo peel for removal of brilliant green and crystal violet. *Journal of Chemical Research, 49*(3). https://doi.org/10.1177/17475198251351169

Hoang, B.N., Nguyen, M.L., Hoang, M.A. & Doan, Q.M.T. (2024). Green synthesis of ϒ- Fe_2O_3 using orange peel extract and application to remove Congo red. *Journal of Chemical Research, 48*(6). https://doi.org/10.1177/17475198241301476

https://goldbook.iupac.org/terms/view/P04775 'Potential at the point of zero charge' In *The IUPAC Compendium of Chemical Terminology*. International Union of Pure and Applied Chemistry. https://doi.org/10.1351/goldbook.P04775

Jawed, A., Golder, A.K. & Pandey, L.M. (2023). Synthesis of iron oxide nanoparticles mediated by Camellia sinensis var. Assamica for Cr(VI) adsorption and detoxification. *Bioresource Technology*, 376, 128816. https://doi.org/10.1016/j.biortech.2023.128816

Jegadeesan, G.B., Srimathi, K., Santosh Srinivas, N., Manishkanna, S. & Vignesh, D. (2019). Green synthesis of iron oxide nanoparticles using terminalia bellirica and moringa oleifera fruit and leaf extracts: Antioxidant, antibacterial and thermoacoustic properties. *Biocatalysis and Agricultural Biotechnology*, 21. https://doi.org/10.1016/j.bcab.2019.101354

Kahrilas, G.A., Wally, L.M., Fredrick, S.J., Hiskey, M., Prieto, A.L. & Owens, J.E. (2014). Microwave-assisted green synthesis of silver nanoparticles using orange peel extract. *ACS Sustainable Chemistry & Engineering*, *2*(3), 367-376. https://doi.org/10.1021/sc4003664

Kanagasubbulakshmi, S., Kadirvelu, K. (2017). Green synthesis of iron oxide nanoparticles using lagenaria siceraria and evaluation of its antimicrobial activity. *Defence Life Science Journal*, *2*(4), 422. https://doi.org/10.14429/dlsj.2.12277

Kosmulski, M. (2020). The pH dependent surface charging and points of zero charge. VIII. Update. *Advances in Colloid and Interface Science*, 275, 102064. https://doi.org/10.1016/j.cis.2019.102064

Kosmulski, M. (2023). The pH dependent surface charging and points of zero charge. X. Update. *Advances in Colloid and Interface Science*, 319, 102973. https://doi.org/10.1016/j.cis.2023.102973

Lakshmnarayanan, S., Shereen, M.F., Niraimathi, K.L., Brindha, P. & Arumugam, A. (2021). One-pot green synthesis of iron oxide nanoparticles from bauhinia tomentosa: Characterization and application towards synthesis of 1, 3 diolein. *Scientific Reports*, *11*(1), 8643. https://doi.org/10.1038/s41598-021-87960-y

Lam, V.T., Hoang, B. & Quyen, N.T.C. (2023). Effect of microwave-assisted method on antibiotic adsorption capacity of activated carbon from grapefruit. *Advances in Science and Technology*, 122, 57-63. https://doi.org/10.4028/p-0iyi0c

Mahmoudi, G., Sufimahmoudi, E. & Sajadi, S.M. (2020). Bioactive metal oxide nanoparticles from some common fruit wastes and euphorbia condylocarpa plant. *Food Science and Nutrition*, *8*(10), 5521-5531. https://doi.org/10.1002/fsn3.1853

Maiti, D., Mukhopadhyay, S. & Devi, P.S. (2017). Evaluation of mechanism on selective, rapid and superior adsorption of Congo red by reusable mesoporous α-Fe_2O_3 nanorods. *ACS Sustainable Chemistry & Engineering*, *5*(12), 11255-11267. https://doi.org/10.1021/acssuschemeng.7b01684

Mutlu, H., Barner, L. (2022). Getting the terms right: Green, sustainable or circular chemistry? *Macromolecular Chemistry and Physics*, *223*(13), 2200111. https://doi.org/10.1002/macp.202200111

Nasiri, K. (2023). Synthesis of Ag-Fe_2O_3 nanoparticles with anti-bacterial and anti-fungal impacts on dental microbia. *Nanomedicine Research Journal*, *8*(3), 283-289. https://doi.org/10.22034/nmrj.2023.03.007

Nguyen, V.H., Van, H.T., Nguyen, V.Q., Dam, X.V., Hoang, L.P. & Ha, L.T. (2020). Magnetic Fe_3O_4 nanoparticle biochar derived from pomelo peel for reactive red 21 adsorption from aqueous solution. *Journal of Chemistry*, *2020*(1), 3080612. https://doi.org/10.1155/2020/3080612

Noreen, S., Mustafa, G., Ibrahim, S.M., Naz, S., Iqbal, M., Yaseen, M., … & Nisar, J. (2020). Iron oxide (Fe_2O_3) prepared via green route and adsorption efficiency evaluation for an anionic dye: Kinetics isotherms and thermodynamics studies. *Journal of Materials Research and Technology*, *9*(3), 4206-4217. https://doi.org/10.1016/j.jmrt.2020.02.047

Pietrzyk, P., Phuong, N.T., Olusegun, S.J., Hong Nam, N., Thanh, D.T.M., Giersig, M., … & Osial, M. (2022). Titan yellow and Congo red removal with superparamagnetic iron-oxide-based nanoparticles doped with zinc. *Magnetochemistry*, *8*(8), 91. https://doi.org/10.3390/magnetochemistry8080091

Quyen, N.T.C., Van, T.L., Bach, L.G. & Hoang, B.N. (2023). Antibiotic removal capacity of coconut activated carbon from microwave-assisted synthesis. *Key Engineering Materials*, 949, 175-185. https://doi.org/10.4028/p-VfN0Z5

Ramesh, R., Yamini, V., Rajkumar, D., John Sundaram, S., Lakshmi, D. & Khan, F.L.A. (2019). Biogenic synthesis of a-Fe_2O_3 nanoparticles using Plectranthus amboinicus leaf extract. *Materials Today: Proceedings*, 36, 453-458. https://doi.org/10.1016/j.matpr.2020.05.095

Richard, A., Ronal, O.K. (1971). *Handbook of Infrared and Raman Spectra of Inorganic Compounds and Organic Salts: Infrared Spectra of Inorganic Compounds*. Academic Press, 495.

Sarojini, G., Babu, S.V. & Rajasimman, M. (2022). Adsorptive potential of iron oxide based nanocomposite for the sequestration of Congo red from aqueous solution. *Chemosphere*, 287, 132371. https://doi.org/10.1016/j.chemosphere.2021.132371

Satheesh, R., Vignesh, K., Rajarajan, M., Suganthi, A., Sreekantan, S., Kang, M. & Kwak, B.S. (2016). Removal of Congo red from water using quercetin modified α-Fe_2O_3 nanoparticles as effective nanoadsorbent. *Materials Chemistry and Physics*, 180, 53-65. https://doi.org/10.1016/j.matchemphys.2016.05.029

Sathishkumar, G., Logeshwaran, V., Sarathbabu, S., Jha, P.K., Jeyaraj, M., Rajkuberan, C., … & Sivaramakrishnan, S. (2018). Green synthesis of magnetic Fe_3O_4 nanoparticles using couroupita guianensis Aubl. fruit extract for their antibacterial and cytotoxicity activities. *Artificial Cells, Nanomedicine and Biotechnology*, *46*(3), 589-598. https://doi.org/10.1080/21691401.2017.1332635

Sayed, F.N., Polshettiwar, V. (2015). Facile and sustainable synthesis of shaped iron oxide nanoparticles: Effect of iron precursor salts on the shapes of iron oxides. *Scientific Reports*, *5*(1), 9733. https://doi.org/10.1038/srep09733

Shalaby, S.M., Madkour, F.F., El-Kassas, H.Y., Mohamed, A.A. & Elgarahy, A.M. (2021). Green synthesis of recyclable iron oxide nanoparticles using Spirulina platensis microalgae for adsorptive removal of cationic and anionic dyes. *Environmental Science and Pollution Research*, *28*(46), 65549-65572. https://doi.org/10.1007/s11356-021-15544-4

Sithara, N.V., Bharathi, D., Lee, J., Mythili, R., Devanesan, S. & AlSalhi, M.S. (2024). Synthesis of iron oxide nanoparticles using orange fruit peel extract for efficient remediation of dye pollutant in wastewater. *Environmental Geochemistry and Health*, *46*(2).

https://doi.org/10.1007/s10653-023-01781-8

Song, M., Yang, D., Ramu, A.G. & Choi, D. (2025). 3D porous Fe_2O_3-incorporated basalt filter unit for simultaneous removal of As(III) and As(V) from aqueous solutions: Adsorption isotherm and mechanism. *Environmental Science and Pollution Research, 32*(12), 7722-7736. https://doi.org/10.1007/s11356-025-36170-4

Taghavi, F.S., Ramazani, A., Golfar, Z. & Woo, J. (2017). Green synthesis of α-Fe_2O_3 (hematite) nanoparticles using tragacanth gel. ResarchGate.

Van Hung, P., Anh, M.N.T., Hoa, P.N. & Phi, N.T.L. (2021). Extraction and characterization of high methoxyl pectin from citrus maxima peels using different organic acids. *Journal of Food Measurement and Characterization, 15*(2), 1541-1546. https://doi.org/10.1007/s11694-020-00748-y

Van Phuoc, N., Quoc, H. Le, Tran, T.T., Van Tan, L. & Hoang, B.N. (2023). Optimization of ciprofloxacin removal by response surface methodology using activated carbon from Burmese grape obtained from Vietnam. *Journal of Chemical Research, 47*(6), 17475198231212143. https://doi.org/10.1177/17475198231212143

Van Tran, T., Bui, Q.T.P., Nguyen, T.D., Ho, V.T.T. & Bach, L.G. (2017). Application of response surface methodology to optimize the fabrication of $ZnCl_2$-activated carbon from sugarcane bagasse for the removal of Cu^{2+}. *Water Science and Technology, 75*(9), 2047-2055. https://doi.org/10.2166/wst.2017.066

Yang, P., Pan, L., Lan, J., Ye, Y., Ao, R., Xie, X., … & Lan, X. (2025). Adsorption performance of Fe_2O_3-modified dolomite composite (DFC) for Congo red removal. *Water, 17*(8), 1198. https://doi.org/10.3390/w17081198

Yarmohammadi, N., Ghadermazi, M., Derikvand, Z. & Mozafari, R. (2022). In situ synthesis of bimetallic γ-Fe_2O_3/Cu nanoparticles over pectin hydrogel obtained from biomass resource (orange peel) as a reusable green catalyst for oxidation and C-S cross-coupling reactions. *Chemical Papers, 76*(7), 4289-4307. https://doi.org/10.1007/s11696-022-02174-4

Yesmin, S., Mahiuddin, Md., Nazmul Islam, A.B.M., Karim, K.M.R., Saha, P., Khan, Md.A.R. & Ahsan, H.Md. (2024). Piper chaba stem extract facilitated the synthesis of iron oxide nanoparticles as an adsorbent to remove Congo red dye. *ACS Omega, 9*(9), 10727-10737. https://doi.org/10.1021/acsomega.3c09557

Zhu, L., Sana, A., Qamar, M.T., Bahadur, A., Liu, G., Aslam, M., … & Alotaibi, K.M. (2025). Response surface methodology for the design of malachite green dye removal by γ-Fe_2O_3 dispersed on reduced graphene oxide sheets. *Scientific Reports, 15*(1), 4402. https://doi.org/10.1038/s41598-025-88072-7